J. Fluid Mech. (1989), *vol.* 207, *pp.* 505–529
Printed in Great Britain

Slow spreading of a sheet of Bingham fluid on an inclined plane

By KO FEI LIU AND CHIANG C. MEI

Parsons Laboratory, Department of Civil Engineering, Massachusetts Institute of Technology, Cambridge, MA 02139, USA

(Received 2 March 1987 and in revised form 13 January 1989)

To study the dynamics of fluid mud with a high concentration of cohesive clay particles, we present a theory for a thin sheet of Bingham-plastic fluid flowing slowly on an inclined plane. The physics is discussed on the approximate basis of the lubrication theory. Because of the yield stress, the free surface need not be horizontal when the Bingham fluid is in static equilibrium, nor parallel to the plane bed when in steady flow. We then show that there is a variety of gravity currents that can advance at a constant speed and with the same profile. Experimental confirmation of one type is presented. By solving a nonlinear partial differential equation, transient flows due either to a steady upstream discharge or to the sudden release of a finite fluid mass on another fluid layer are studied. In the first case there is a mud front which ultimately propagates as a constant speed as a steady gravity current. In the second case, when the ambient layer is sufficiently shallow that there is no initial motion, the flow induced by the new fluid can terminate after the disturbance has travelled a finite distance. The extent of the final spread is examined. Disturbances due to an external pressure travelling parallel to the free surface are also examined. It is found in particular that a travelling localized pulse of pressure gradient not only generates a localized mud disturbance which travels along with the forcing pressure, but further leaves behind a permanent footprint.

1. Introduction

It is known that some fluids such as paint, volcanic lava or water with a high concentration of cohesive clay particles behave approximately as Bingham plastic. In simple shear, the stress–strain relation is nonlinear:

$$\mu\frac{\partial u}{\partial z}=\begin{cases}0 & \text{if } |\tau|<\tau_0\\ \tau-\tau_0\operatorname{sgn}\dfrac{\partial u}{\partial z} & \text{if } |\tau|>\tau_0\end{cases}, \tag{1.1}$$

where τ_0 is the yield stress and μ the coefficient of viscosity. This is the simplest idealization of a shear-thinning pseudo-plastic fluid whose coefficient of viscosity decreases with the strain rate. In muddy water, both τ_0 and μ increase with clay concentration (Krone 1963; Migniot 1968). Because of the nonlinear relation above, analysis of the transient mechanics of Bingham fluids is difficult. As an example, it was not until recently that Phan-Thien (1983) found the exact solution to the Rayleigh problem for the flow induced by a suddenly imposed constant stress at the bottom of a half-space. Approximate numerical methods for some one-dimensional unsteady shear flows in an infinitely deep fluid have been developed by Makarov &

Sal'nikov (1973) and Makarov, Zhdanova & Plolzova (1974). But the recent survey by Bird, Dai & Yarusso (1983) shows a preponderance of steady flow solutions. For two dimensions the numerical method of finite elements has been developed by Bercovier & Engelman (1980) for steady flows, but not yet extended to transient flows. A recent review of numerical methods for non-Newtonian fluids in general have been given by Crochet & Walters (1983) and Crochet, Davies & Walters (1984). Theoretical treatments of free-surface flows of a Bingham fluid, either analytical or numerical, are scarce in the published literature.

On the other hand, there have been a large number of papers on free-surface flows of Newtonian viscous fluids, motivated by various scientific and technical reasons. These include the linearized instability analyses of a thin sheet down an incline (Yih 1954, 1963; Benjamin 1957), and extensions to nonlinear instabilities (Lin 1969, 1974). There are also nonlinear theories of gravity currents which may be regarded as transient long waves of finite amplitude (Batchelor 1967, p. 263; Benney 1966; Mei 1966). In particular, when the wave amplitude is comparable with the layer depth, the leading-order equation governing the depth is a diffusion equation with diffusivity proportional to the third power of the unknown concentration. This approximation has been extended to axisymmetric spreading of a viscous current and to two-layered fluids by Huppert (1982*a*, *b*). The predicted spreading rates agree well with the experiments by Didden & Maxworthy (1982) and by Huppert (1982*b*) who also discussed geological applications to the spreading of lava domes (Huppert 1986). Mei's (1966) study includes waves of intermediate amplitudes and the effects of frequency dispersion, and predicts the existence of polyclinal permanent waves. Similar analyses of transient free surface flows of Bingham fluids appear wanting.

Our impetus for studying Bingham fluids is to seek physical understanding of the evolution of a muddy coast. Cohesive clay particles are carried in suspension to the sea by river flows, and settle to the bottom upon entering the sea. By currents, tides, surface waves or its own weight, mud spreads along the coast and into the deeper sea. This spreading contributes to the transformation of muddy coasts and is a slow process that may take months or years. Because fluid mud is known to have strong non-Newtonian properties at high concentration (see e.g. Williams 1980; Verreet & Berlamont 1987; Mei & Liu 1987 and references therein), it is worth studying how this property affects mud spreading under various types of forcing. It is, however, useful to emphasize that our knowledge of the constitutive behaviour of hyperconcentrated fluid mud is far from comprehensive. Under low stress, this material may behave as a viscoelastic solid (McPherson 1980; Mehta & Maa 1987). Only under sufficiently high stress does it behave approximately as a Bingham-plastic fluid, with some thixotropic tendency. The viscosity and yield stress vary widely depending on concentration and chemical composition. For example, Migniot (1968) found in Provins Estuary, France, that $\mu = O(10)$ gm/cm and $\tau_0 = O(100)$ dynes/cm^2 for a concentration of 0.4 gm/cm^3. In the Yellow River of China where the clay concentration can be as high as 1.5 gm/cm^3, the values are much greater (Wang *et al.* 1985). Little systematic information is available on the transitional regime from possibly viscoelastic to Bingham-plastic behaviour. Despite the lack of precise details, qualitative descriptions by many observers that fluid mud at rest is like gel or yogurt suggest that under low stress, fluid mud is closer to a viscoelastic solid than a Newtonian fluid; the internal shear stress must exceed a certain threshold for permanent rate of shearing to occur. In §§2–7 we examine the idealized model of Bingham plastic and study the slow spreading of a thin fluid layer due to gravity or externally applied pressure. Under the assumptions that the fluid is

homogeneous, the flow is of the low-Reynolds-number type, the wavelength is much greater than the depth, and the wave amplitude is allowed to be comparable with depth, the approximate equation is derived. Because of the yield stress, the free surface can possess a rich variety of configurations either in static or dynamic equilibrium. The states of static equilibrium corresponding to thresholds of motion are first discussed; these configurations are the final states of transient motion to be examined later. Several new types of steady gravity currents which can propagate at a constant speed without change of form are then presented. For transient flows the governing equation which contains both diffusive and convective terms and is subject to an inequality constraint is then solved numerically. If a given mass of fluid is released on a layer of stationary fluid, the induced motion is shown to stop after the front has travelled a finite distance. This is very different from Newtonian fluids which can only slow down but can never stop. The final extent of spreading is calculated as a function of the initial volume of the released fluid mass. As a final example, the effect of a travelling pulse of surface pressure, which can be caused by a cylinder travelling slowly above a muddy sea bed, is also examined. An effect of the yield stress is manifested in the presence of a permanent footprint left behind by the moving pressure pulse.

2. Shallow-water approximation

Consider a single layer of fluid flowing down a plane inclined clockwise at the angle θ with respect to the horizon (see figure 1). Let the x-axis coincide with the plane bed and be directed downward. The free surface is designated as $z = h(x,t)$. The characteristic lengthscale along the bed is assumed to be so much greater than the fluid depth that the pressure within is hydrostatic, i.e.

$$p = \rho g(h-z)\cos\theta + P(x,t), \tag{2.1}$$

where $P(x,t)$ denotes the externally applied pressure, and the velocity is essentially in the x-direction. i.e. $u \gg v$. Throughout the entire fluid layer the balance of longitudinal momentum requires

$$0 = \rho g \sin\theta - \frac{\partial p}{\partial x} + \frac{\partial \tau}{\partial z}, \quad 0 \leqslant z \leqslant h \tag{2.2}$$

so that the stress increases linearly with depth,

$$\tau = -(h-z)\left[\frac{\partial P}{\partial x} - \rho g\cos\theta\left(\tan\theta - \frac{\partial h}{\partial x}\right)\right]. \tag{2.3}$$

At the bed, $z = 0$, the stress is

$$\tau_b = -h\left[\frac{\partial P}{\partial x} - \rho g\cos\theta\left(\tan\theta - \frac{\partial h}{\partial x}\right)\right]. \tag{2.4}$$

Clearly $|\tau_b|$ must exceed τ_0 for fluid to move. In particular, the fluid moves $\begin{pmatrix}\text{downward}\\ \text{upward}\end{pmatrix}$ if

$$\pm\frac{\tau_0}{h} \leqslant -\frac{\partial P}{\partial x} + \rho g\cos\theta\left(\tan\theta - \frac{\partial h}{\partial x}\right). \tag{2.5}$$

Whenever $|\tau_b| < \tau_0$, or

$$\tau_0 > h\left[-\frac{\partial P}{\partial x} + \rho g\cos\theta\left(\tan\theta - \frac{\partial h}{\partial x}\right)\right] > -\tau_0 \tag{2.6}$$

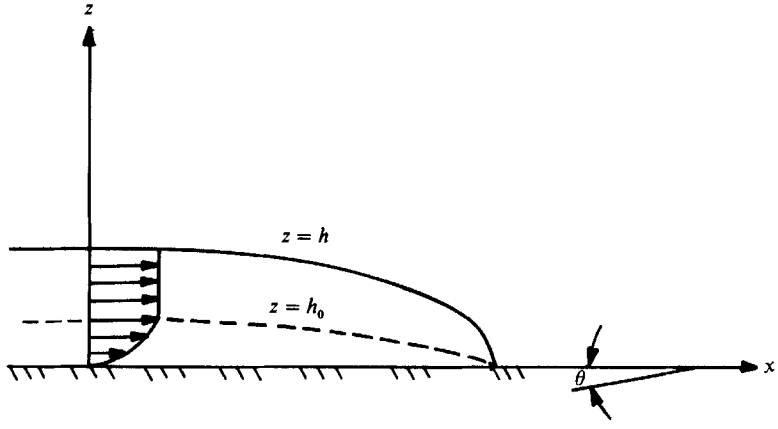

FIGURE 1. A layer of fluid mud on a sloping bed.

the mud does not move at all. When $\tau_b = \tau_0$ (or $-\tau_0$) the mud is at the threshold of downward (or upward) flow.

When (2.5) is satisfied there is a yield surface at $z = h_0 < h$ where $|\tau| = \tau_0$. Below the yield surface, $0 < z < h_0$, there is shearing. Equation (2.2) reads

$$0 = \rho g \sin\theta - \frac{\partial p}{\partial x} + \mu \frac{\partial^2 u}{\partial z^2} \tag{2.7}$$

with the conditions

$$u = 0, \quad z = 0 \tag{2.8}$$

and

$$\frac{\partial u}{\partial z} = 0, \quad z = h_0. \tag{2.9}$$

It follows that

$$u = \frac{1}{\mu}\left[\frac{\partial P}{\partial x} - \rho g \cos\theta\left(\tan\theta - \frac{\partial h}{\partial x}\right)\right](\tfrac{1}{2}z^2 - h_0 z), \quad 0 \leqslant z \leqslant h_0. \tag{2.10}$$

Above the yield surface there is a layer of plug flow within which $u = u_p$ is independent of z. Matching u_p with (2.10) at $z = h_0$ we get

$$u_p = -\frac{h_0^2}{2\mu}\left[\frac{\partial P}{\partial x} - \rho g \cos\theta\left(\tan\theta - \frac{\partial h}{\partial x}\right)\right], \quad h_0 \leqslant z \leqslant h. \tag{2.11}$$

On the yield surface, $\tau = \pm\tau_0$. It follows from (2.3) and (2.10) that

$$\tau_0 \operatorname{sgn} u = -(h - h_0)\left[\frac{\partial P}{\partial x} - \rho g \cos\theta\left(\tan\theta - \frac{\partial h}{\partial x}\right)\right]. \tag{2.12}$$

The total volume flux at any station is clearly

$$q = \int_0^{h_0} u\,dz + u_p(h - h_0) = -\frac{1}{6\mu}\left[\frac{\partial P}{\partial x} - \rho g \cos\theta\left(\tan\theta - \frac{\partial h}{\partial x}\right)\right] h_0^2(3h - h_0). \tag{2.13}$$

Conservation of mass in the entire fluid layer requires

$$\frac{\partial h}{\partial t} + \frac{\partial q}{\partial x} = 0. \tag{2.14}$$

Equations (2.12), (2.13) and (2.14) are the governing equations for the three unknowns $h(x,t)\, h_0(x,t)$ and $q(x,t)$.

In the limit of $\partial P/\partial x = 0$ and Newtonian fluids, $h_0 = h$; (2.13) and (2.14) can be easily combined to yield the known result (Mei 1966; Batchelor 1967; Huppert 1982*b*)

$$\frac{\partial h}{\partial t}+\frac{g}{\nu}\cos\theta\frac{\partial}{\partial x}\left[\left(\tan\theta-\frac{\partial h}{\partial x}\right)\frac{h^3}{2}\right]=0. \tag{2.15}$$

As an elementary example showing a special consequence of the yield stress, a uniform layer with an unpressurized free surface is at the threshold of downward flow, if $\tau_b = \tau_0$. This occurs when

$$h = \bar{h} = \frac{\tau_0}{\rho g \sin\theta} \tag{2.16}$$

from (2.5). Thus a uniform mud layer can remain stationary on an incline if $h < \bar{h} \neq 0$, in sharp contrast to a Newtonian fluid.

We now introduce normalized variables for the general case

$$(z, h, h_0, H) = \bar{h}(z', h', h_0', H'), \tag{2.17a}$$

$$x = \bar{h}\cot\theta x', \quad t = \frac{\mu}{\tau_0}\cot\theta t', \tag{2.17b}$$

$$(u, u_p) = \frac{\tau_0}{\mu}\bar{h}(u', u_p'), \tag{2.17c}$$

$$q = \frac{\tau_0}{\mu}\bar{h}^2 q', \quad P = \rho g \bar{h} P'. \tag{2.17d}$$

With (2.17) equations (2.10) and (2.13) become, with primes omitted,

$$u = \begin{cases} -\left(-\dfrac{\partial P}{\partial x}+1-\dfrac{\partial h}{\partial x}\right)[\tfrac{1}{2}z^2 - h_0 z], & 0 \leqslant z \leqslant h_0 \\ u_p, & h_0 \leqslant z \leqslant h, \end{cases} \tag{2.18}$$

$$q = \frac{1}{6}\left(-\frac{\partial P}{\partial x}+1-\frac{\partial h}{\partial x}\right)h_0^2(3h-h_0), \tag{2.19}$$

while (2.14) is unchanged.

In the normalized variables the horizon has the slope $\partial h/\partial x = 1$. From (2.12) and (2.17) the normalized plug flow depth is

$$h - h_0 = \left(-\frac{\partial P}{\partial x}+1-\frac{\partial h}{\partial x}\right)^{-1}\operatorname{sgn}(u). \tag{2.20}$$

The region of no motion is defined from (2.6) by

$$\frac{1}{h} \geqslant -\frac{\partial P}{\partial x}+1-\frac{\partial h}{\partial x} \geqslant -\frac{1}{h}. \tag{2.21}$$

Note that this normalization is valid only for small slope, because the long-wave assumption implies $\theta \ll 1$ from (2.17*b*).

Similarly to the case of a Newtonian fluid spreading on a horizontal bed (Huppert 1982*a*), the equations obtained here can be applied to a fluid mud layer immersed at the bottom of a shallow layer of stationary clear water of density ρ_w with much smaller viscosity, if g is replaced by the reduced gravity $g(\rho-\rho_w)/\rho$. A condition for this to hold is that the water layer is sufficiently deep that the bottom disturbance cannot be felt on the free surface. This requires that the depth of water is greater

than the length of waves $O(u^2/g)$ that may otherwise be generated by a disturbance travelling at the speed u. This condition is assumed from here on. The pressure P can be regarded as the consequence of a moving submarine or atmospheric pressure. Strictly speaking, such disturbances induce coupled motions in both water and mud layers. But as long as we restrict our interest to the physics in the mud layer, much can be learned by prescribing the associated pressure distribution on the water/mud interface. This simplified view will be adopted here.

Lastly we give some estimates of the magnitudes involved in a typical muddy seabed. Take the clay concentration to be around 15% by volume. The density of fluid mud is then $\rho = 1.2$ g/cm^3 while $\tau_0 = 30$ dynes/cm^2 and $\mu = 50$ g/cm s. On a bed of slope $\theta = 1°$, the reduced gravity is $g' = 163$ cm/s^2, $\bar{h} = 8.8$ cm; the scales of x, t and u are 503 cm, 95.5 s and 5.3 cm/s respectively. By using the reasoning in the usual lubrication theory, the pertinent Reynolds number can be shown to be $R_e = \rho\tau_0\bar{h}^2\tan\theta/\mu^2$ since the characteristic velocity here is $\tau_0\bar{h}/\mu$ and the ratio of transverse to longitudinal lengthscales is $\tan\theta$. For the values just cited this Reynolds number is about 0.016, which is small enough to omit inertia, as we have done here.

3. Profiles of a stationary layer on the threshold of motion

Because of the finite yield stress, the fluid depth need not be uniform for a layer to be in static equilibrium. Since these non-trivial surface shapes can be related to the final state when the fluid comes to rest, it is useful to discuss them first. In this section we assume that there is no applied surface pressure ($P = 0$).

In the special case of a horizontal bottom, the threshold profiles follow most directly from (2.6) with the equality sign. With $P = \theta = 0$, the surface profile is, in physical variables:

$$h^2 - h_*^2 = \pm\frac{2\tau_0}{\rho g}(x - x_*), \tag{3.1}$$

where $h = h_*$ at $x = x_*$. The upper (or lower) sign corresponds to a parabolic head facing the left (or right).

For any finite bed slope, we turn to the dimensionless equation (2.21) with the equality signs. With any disturbance mud will start to move

$$\left.\begin{matrix}\text{downward}\\ \text{upward}\end{matrix}\right\} \quad \text{if} \quad \left\{\frac{dh}{dx} = 1 \mp \frac{1}{h}\right. . \tag{3.2}$$

Therefore we refer the upper (lower) sign in (3.2) to the downward (upward) threshold profiles respectively. Corresponding to (2.16), $h = 1$ is a special solution of (3.2), as represented by the straight line (a) in figure 2. Consider a general downward threshold profile. Equation (3.2) with the upper sign can be integrated to give

$$h - h_* + \ln\frac{h-1}{h_*-1} = x - x_*. \tag{3.3}$$

Now we must distinguish the two cases $h_* < 1$, or > 1; $h_* = 1$ corresponds to the trivial limit of $h = 1$. For $0 < h_* < 1$, the depth is everywhere less than the critical uniform depth and approaches unity as $x \to -\infty$. A typical profile is shown as curve (b) in figure 2 for $h_* = 0$ at $x = x_* = 0$, depicting the front of mud layer about to flow down a dry bed. The slope is infinite at the front $x = x_* - h_* - \ln(1 - h_*)$ where the bed is dry. A more refined theory is in principle needed for this neighbourhood but is not pursued here.

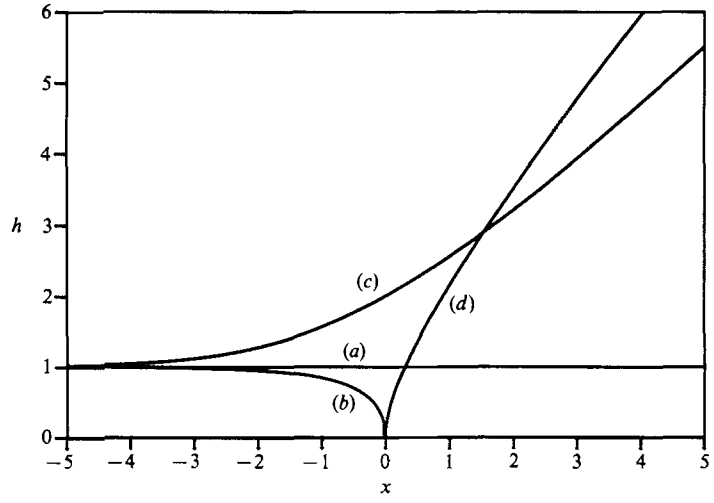

FIGURE 2. Threshold profiles on a sloping bed. Curve (*a*) A uniform layer about to move down. (*b*) The head of a uniform layer about to move down. (*c*) A mud sea which has just stopped sinking. (*d*) A mud sea which has just stopped rising.

If $h_* > 1$ then the depth increases from $h = 1$ at $x \sim -\infty$ to ∞ at $x \sim +\infty$ where the mud surface is horizontal. (Recall that the asymptotic slope of 1 corresponds to the horizon in the physical plane.) In this case the bed can be considered as the left bank of a large reservoir on the threshold of draining. A typical profile for $h_* = 2$ at $x = x_* = 0$ is plotted in figure 2 as curve (*c*).

Similarly the upward threshold profile is given by

$$h - h_* - \ln\frac{1+h}{1+h_*} = x - x_*. \tag{3.4}$$

The depth increases monotonically from 0 at $x = x_* - h_* + \ln(1+h_*)$ to ∞ at $x \sim \infty$, as shown by curve (*d*) for $h_* = 0$ at $x_* = 0$ in figure 2. This corresponds to a mud reservoir at the threshold of rising; any disturbance would induce upward motion.

The case of non-zero external pressure involves more physical aspects and will be discussed later.

4. Permanent waves with no external pressure

4.1. *Theory*

If from $t = 0$ onwards fresh mud is steadily discharged at an upstream station of a slope, we expect a gravity current down the slope which finally propagates at a constant speed C. The solution near the front depends ultimately on x and t in the form

$$h = h(X), \quad h_0 = h_0(X), \quad q = q(X), \tag{4.1}$$

where

$$X \equiv x - Ct. \tag{4.2}$$

This type of solution is called *permanent waves* in water wave theory. Mathematically it is the most elementary wave in a nonlinear system, just as the simple harmonic progressive wave is in a linear system. For a Bingham fluid the variety of such waves is large as we shall now discuss.

Equation (2.14) can be integrated at once to give

$$q = C(h-h_e), \tag{4.3}$$

where $h_e \geqslant 0$ is an integration constant.

With this and $\partial P/\partial x = 0$, (2.19) and (2.20) become

$$C(h-h_e) = \frac{1}{6}\left(1-\frac{dh}{dX}\right)h_0^2(3h-h_0) \tag{4.4}$$

and

$$1-\frac{dh}{dX} = \frac{\text{sgn}\,(u)}{h-h_0}. \tag{4.5}$$

For given parameters C and h_e, h_0 can in principle be eliminated from (4.4) and (4.5) to give a first-order nonlinear ordinary differential equation for h:

$$F\left(\frac{dh}{dX}, h, X; C, h_e, \text{sgn}\,(u)\right) = 0. \tag{4.6}$$

By examining various ranges of C and h_e, several types of permanent waves (gravity currents) can be found.

Case I. Downward propagation ($C > 0$) *and downward flow* ($q > 0$)

(i) *Gravity current connecting two uniform layers.* The simplest kind of permanent wave with downward flow is a gravity current connecting a uniform depth h_{max} upstream to another uniform depth h_{min} downstream. At each extreme, $X \to \pm\infty$, $dh/dX = 0$. From (4.4) and (4.5) we get

$$h^3 - \tfrac{3}{2}h^2 - 3C(h-h_e) + \tfrac{1}{2} = 0, \tag{4.7}$$

$$h = h_0 + 1, \tag{4.8}$$

for $X \to \pm\infty$. In figure 3, h is plotted as a function of h_e for various C, in accordance with (4.7). For any $C > 0$ and $1 < h_e < h_e^*$ with

$$h_e^* = \frac{1}{2} - \frac{1}{12C} + \left(\frac{1}{12C}+\frac{1}{3}\right)(1+4C)^{\frac{1}{2}} \tag{4.9a}$$

and the corresponding depth

$$h^* = \tfrac{1}{2}[1+(1+4C)^{\frac{1}{2}}], \tag{4.9b}$$

(4.7) has two roots h_{max} and h_{min}, both of which are greater than unity. By substituting $h = h_{max}$ and h_{min} in turn in (4.7) and eliminating h_e we find the relation

$$C = \tfrac{1}{3}(h_{max}^2 + h_{max}h_{min} + h_{min}^2) - \tfrac{1}{2}(h_{max}+h_{min}), \quad h_{min} \geqslant 1. \tag{4.10}$$

This relation between the phase speed and the layer depths is plotted in figure 4.

If however $0 < h_e < 1$, there is only one root of (4.7); $h_{max} > 1$. From (4.3) $h_{min} = h_e$ where $q = 0$. Thus $q > 0$ for $X < 0$ and $q = 0$ for $X \geqslant 0$ and the gravity current propagates downward from a thicker flowing layer of depth h_{max} to a thinner stationary layer of depth $h_{min} = h_e$. At the moving front of the gravity current where $q = 0$, mud is liquified. From (4.7) we get

$$C = \frac{(h_{max}-1)^2(h_{max}+\frac{1}{2})}{3(h_{max}-h_{min})}, \quad h_{min} \leqslant 1. \tag{4.11}$$

Equation (4.11) is also plotted in figure 4.

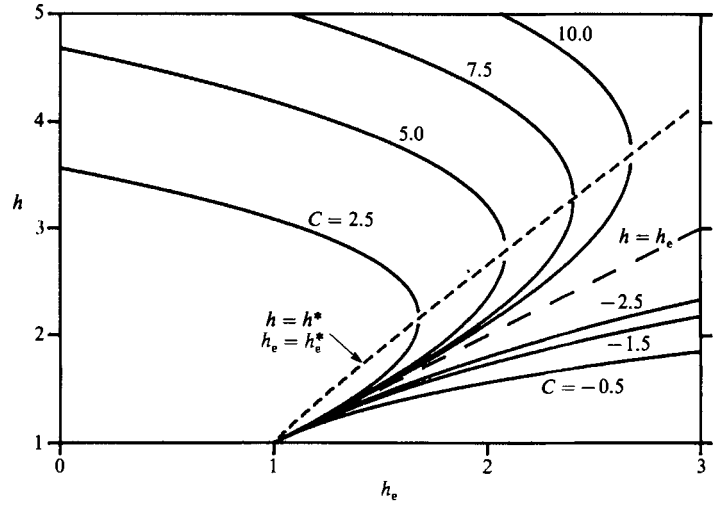

FIGURE 3. Depth h of uniform flow as a function of C and h_e. -----, $h_e = h_e^*$ and $h = h^*$ (cf. (4.9*a*, *b*)).

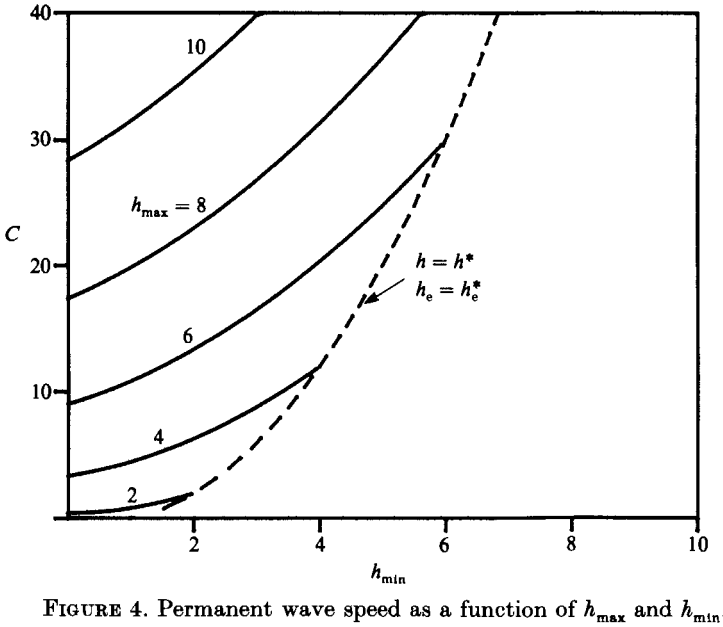

FIGURE 4. Permanent wave speed as a function of h_{max} and h_{min}.

In either case, once $C(>0)$ and h_e are prescribed, h_{max} and h_{min} are fixed. The profile $h(X)$ can be numerically integrated from (4.6) (or (4.4) and (4.5)). By assigning the initial condition that $h(X_1) = h_i < h_{max}$ for some convenient X_1, we can integrate towards $X \sim \infty$ (or $-\infty$) to obtain the downstream (or upstream) part of the profile. A different choice of h_i for a fixed X_i amounts to a shift of origin and is immaterial. For an initial depth close to a uniform flow $h = h_{max} + h_1$, where h_1 can be of either sign and $|h_1| \ll h_{max}$, we can obtain the corresponding change in dh/dX from (4.4) and (4.5). The result, to leading order, is

$$\frac{dh}{dX} = \frac{dh_1}{dX} \approx Kh_1, \quad \text{where} \quad K = 3\frac{h_{max}^2 - h_{max} - C}{h_{max}^3 - 1}. \tag{4.12}$$

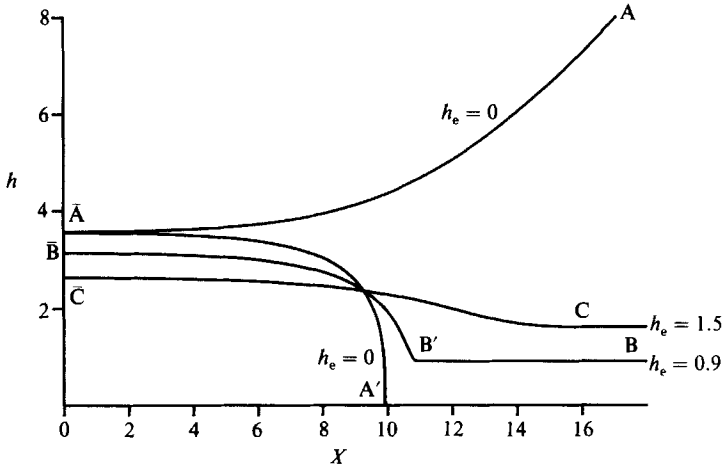

FIGURE 5. Surface profiles of permanent waves corresponding to $C = 2.5$. The values of h_e are marked.

The depth h^* given by (4.9*b*) is the positive root of the numerator of K. Therefore, we find $K > 0$ for $h_{\max} > h^*$, corresponding to the upper branches in figure 3. Consider now $h_1 < 0$, h decreases with X initially from (4.12). Once $\mathrm{d}h/\mathrm{d}X$ starts to decrease, there are two possibilities. One is that it approaches zero; in this case a smaller uniform depth is approached. The other is that h goes to h_e (a non-moving mud layer) or zero (dry bed).

In figure 5, profiles $\bar{A}A'$, $\bar{B}B'B$ and $\bar{C}C$ are obtained for $C = 2.5$, $X_i = 0$ and $h_1 = -0.01$. In particular, for $\bar{C}C$, we choose $h_e = 1.5$ and find from (4.7) that $h_{\max} = 2.66$ and $h_{\min} = 1.60$ (see figure 3). For the same $C = 2.5$, but $h_e = 0.9$, $\bar{B}B'B$ corresponds to a gravity current with $h_{\max} = 3.15$. The downstream portion $B'B$ of the wave front is a stationary mud bed of depth $h_{\min} = h_e = 0.9$. As a special limit $\bar{A}A'$ is the profile for $h_e = 0$, representing a mud current advancing down a dry bed.

(ii) *Uniform layer flowing down into a mud sea.* For prescribed $C > 0$ and $0 < h_e < 1$, we can integrate (4.6) (or (4.4) and (4.5)) by starting from $X = X_i$ with an initial value $h_{\max} + h_1$. However, we now choose $h_1 > 0$. According to (4.12) $\mathrm{d}h/\mathrm{d}X > 0$ and h increases with X at the start. Because there is no uniform flow solution with depth greater than $h_{\max}$, $\mathrm{d}h/\mathrm{d}X$ cannot be zero for any other X. Therefore, h increases with X monotonically.† At the limit of $h \to \infty$, $\mathrm{d}h/\mathrm{d}X \to 1$, which corresponds to a horizontal free surface in natural coordinates. With $X_i = 0$ and $h_1 = 0.01$, a sample profile for $C = 2.5$ and $h_e = 0$ is shown as $\bar{A}A$ in figure 5 which corresponds to $h_{\max} = 3.56$ (see figure 3) and represents the draining of mud along a sloping bank from a uniform layer down to a mud sea.

4.1.2. *Case II. Upward propagation* ($C < 0$)

(i) *Mud sea rising along a sloping uniform layer which is stationary.* We now consider the possibility of an upward-propagating wave front and upward flow ($C < 0$, $q \leqslant 0$). For upward flow ($\mathrm{sgn}(u) = -1$), there is no uniform flow from (4.5) because h must be greater than h_0. But an upward wave can propagate on a stationary bed.

† For this case, $h_{\max}$ is just the real root of (4.7) and corresponds actually to the minimum depth of the whole profile.

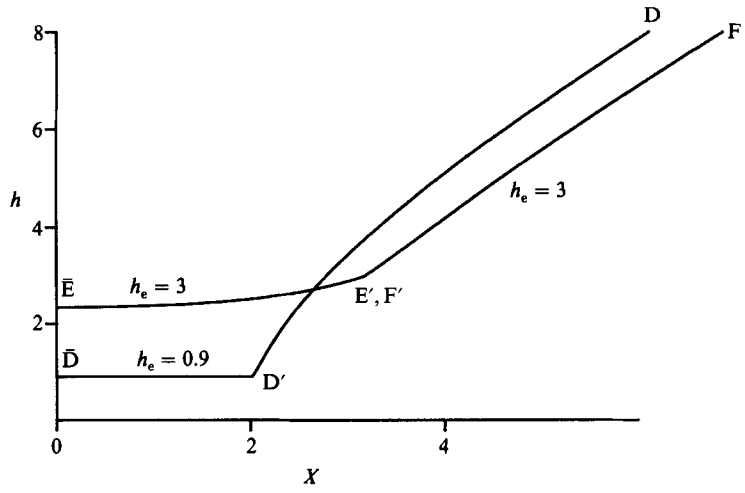

FIGURE 6. Surface profiles of permanent waves corresponding to $C = -2.5$. The values of h_e are marked. ĒE′F′F is the combination of two different curves.

In this case $h = h_e < 1$ and $q = 0$ to the left of the wave front. We can then choose some point X_i as the head of the non-uniform layer downstream and then integrate (4.6) (with $\text{sgn}(u) = -1$) toward $X \sim \infty$. From (4.5) it is easily seen that $dh/dX > 1$ always so that the depth increases monotonically. In figure 6 the profile D̄D′D is calculated with $h_e = 0.9$, $C = -2.5$ and $X_i = 2$. It represents the surface of a mud sea rising along a sloping bank on which lies a uniform layer of stationary mud.

(ii) *Mud sea rising against a downward-flowing mud layer on a sloping bank.* The most complex permanent wave is the combination of two simple flows. On the left of $X_0 (X < X_0)$, the flow is downward ($q > 0$) and uniform far upstream ($X \sim -\infty$), while on the right ($X > X_0$), the flow is upward ($q < 0$). At the point $X = X_0$ we must have $h = h_e > 1$ and $q = 0$. The combined profile propagates upward at the same phase speed $C < 0$.

Note first that for a gravity current with $C < 0$, $q < 0$ and with a uniform depth $h_{\min} > 1$ far upstream, we find from (4.4) and (4.5) by letting $dh/dX = 0$ and $\text{sgn}(u) = 1$ that $h_{\min}$ satisfies (4.7). The results for $h_{\min}$ as a function of h_e are shown in figure 3 for $C = -0.5$, -1.5 and -2.5.

The combined profile can be calculated from (4.6) with $\text{sgn}(u) = \pm 1$ for $X \lessgtr X_0$. We illustrate this by an example for $h_e = 3$ and $C = -2.5$. The corresponding $h_{\min}$ is found from (4.7) to be 2.33. By integrating (4.4) and (4.5) from $X = 0$ with $h(0) = 2.34$ until $h = h_e = 3$ we obtain the profile ĒE′ shown in figure 6. To the right of E′, $\text{sgn}(u) = -1$ in (4.5). Upon integration of (4.4) and (4.5) toward $X \sim +\infty$, we obtain the profile F′F. Therefore, the entire wave form corresponds to a mud sea rising against a downward flowing layer which has a uniform depth far at $X \sim -\infty$.

Finally, for a Newtonian fluid, there can be only two types of gravity currents, under the present scheme of approximation. They correspond to curves C̄C and ĀA′ in figure 5 (see Mei 1966). Therefore more can exist in a Bingham-plastic fluid. These types, and no others, were first found by a more exhaustive examination of the phase portraits of the differential equation (4.6) (or (4.4) and (4.5)).

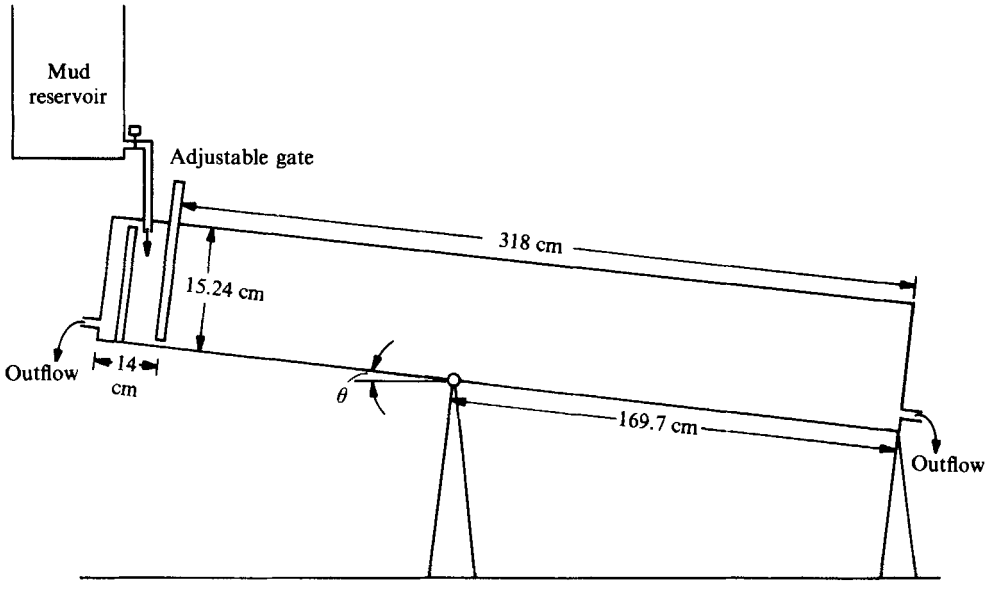

FIGURE 7. Experimental set-up for gravity currents down a dry bed.

4.2. *Experiments on permanent waves down a dry bed*

As a partial check on our theory, we have carried out a simple experiment in the laboratory for one type of permanent wave which flows down an inclined dry bed (cf. $\bar{A}A'$ in figure 5).

The experiments were performed in a Plexiglas tank of 7.62 cm width, 15.24 cm height and 332 cm length as sketched in figure 7. Kaolinite is mixed with tap water to simulate mud. After the mixture is well stirred for 20 minutes, it is put in a reservoir located high above the tilted tank and then discharged at a fixed rate through an adjustable gate. A camera is set up beside the tank 160 cm downstream of the gate and records the mud profile at prescribed instants of time at intervals ranging from 0.5 s to 10 s. After 20–30 frames the camera is relocated at another point further downstream and another set of photographs is taken at known instants of time. At the same time, a stop watch is also used to measure the averaged phase speed of mud as a check. We only analyse those photographs in which the gravity current has reached a steady state.

For rheological properties, a mud sample is taken from the tank. A Brookfield LVT viscometer was used which has four different spindles (with radius $R = 0.942$, 0.513, 0.299, 0.159 cm and length $L = 6.51$, 5.40, 4.29, 3.10 cm respectively) and eight different rotating speeds ranging from 0.3 r.p.m. to 60 r.p.m. The mud sample is put into a cylindrical container with inner radius 4.65 cm and depth 12 cm. For a prescribed rotating speed Ω, the torque T is recorded at the steady state.

For a strictly Bingham plastic and infinitely long spindle and container, the relation between τ_0, μ, T and Ω is known from Bird, Armstrong & Hassager (1987, p. 120) to be

$$2\mu\Omega = -\tau_0 + \tau_0 \ln \tau_0 - \tau_0 \ln \frac{T}{2\pi LR^2} + \frac{T}{2\pi LR^2}. \tag{4.13}$$

This equation holds if there is a zone of stationary fluid near the container wall. This should be the case here because the spindle radius is much smaller than the container

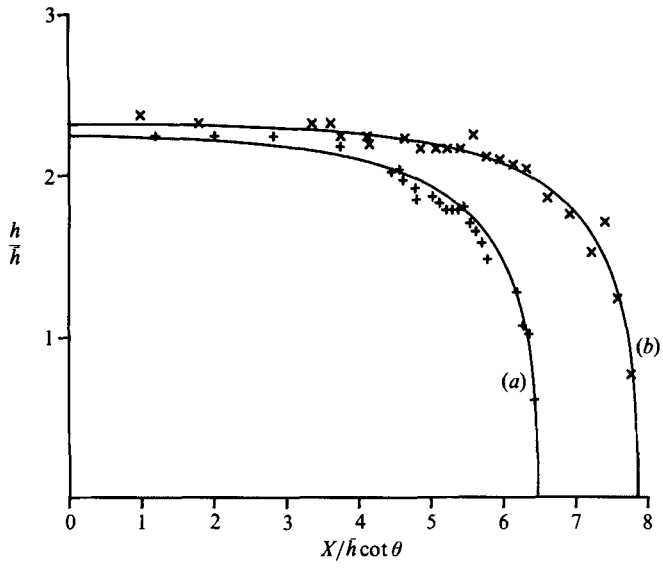

FIGURE 8. Comparison between theory and measured profiles. Curve (*a*) $\theta = 1.47°$, phase speed = 5.22 cm/s, maximum depth = 0.71 cm and $\bar{h} = 0.31$ cm. The corresponding data points are marked +. (*b*) $\theta = 0.90°$, phase speed = 9.46 cm/s, maximum depth = 1.22 cm and $\bar{h} = 0.51$ cm. The corresponding data points are marked ×.

radius. The measured data are then used to find τ_0 and μ by least-square fit with (4.13).

With measured τ_0, μ, ρ and channel slope (θ), we can calculate the physical scales and the normalized phase speed defined in (2.17) for each run. With C and $h_e = 0$ (dry bed), the theoretical wave profiles are obtained by integrating (4.6). The normalized data points for the wave profile are then plotted for comparison.

Good agreement between theory and experiments are found for all runs. Two typical results are shown in figure 8 with the same concentration ($\rho = 1.106$ g/cm^3) but different channel slopes and flow rates. From measurements we get $\tau_0 =$ 8.75 dyne/cm^2 and $\mu = 0.34$ g/cm s. For curve (*a*) in figure 8, $\theta = 1.47°$ and the corresponding Reynolds number $R_e (= \rho\tau_0 h^2 \tan\theta/\mu^2)$ is 0.21. For curve (*b*), $\theta = 1.01°$ and $R_e = 0.38$.

5. Finite-difference scheme for the transient solution

Eliminating h_0 and q from (2.14), (2.19) and (2.20), we get a nonlinear convection–diffusion equation for h:

$$\frac{\partial h}{\partial t} = \frac{1}{3}\left(h^3 \pm \left(1 - \frac{\partial h}{\partial x}\right)^{-3}\right)\frac{\partial^2 h}{\partial x^2} + h\frac{\partial h}{\partial x}\left[h\left(\frac{\partial h}{\partial x} - 1\right) \mp 1\right] \tag{5.1}$$

with the constraint

$$\pm h\left(1 - \frac{\partial h}{\partial x}\right) > 1. \tag{5.2}$$

Again the upper (lower) sign refers to downward (upward) flow. If (5.2) is violated, there is no mud motion. The constraint (5.2) guarantees the diffusivity in (5.1) to be positive. We have chosen the Crank–Nicholson central-difference scheme for the diffusion term in (5.1) and a third-order Adams–Bashforth central difference scheme

for the convective terms. A small artificial viscosity ϵ is introduced to avoid difficulties when the local diffusivity vanishes temporarily:

$$\frac{h_i^{n+1}-h_i^n}{\Delta t}=\frac{1}{6}\left\{(h_i^n)^3\pm\left(1-\frac{h_{i+1}^n-h_{i-1}^n}{2\Delta x}\right)^{-3}+\epsilon\right\}$$
$$\times\left\{\frac{h_{i+1}^{n+1}-2h_i^{n+1}+h_{i-1}^{n+1}}{(\Delta x)^2}+\frac{h_{i+1}^n-2h_i^n+h_{i-1}^n}{(\Delta x)^2}\right\}+\tfrac{23}{12}f_i^n-\tfrac{4}{3}f_i^{n-1}+\tfrac{5}{12}f_i^{n-2}, \quad (5.3)$$

where
$$f_i^n\equiv h_i^n\left(\frac{h_{i+1}^n-h_{i-1}^n}{2\Delta x}\right)\left[h_i^n\left(\frac{h_{i+1}^n-h_{i-1}^n}{2\Delta x}-1\right)\mp 1\right]. \quad (5.4)$$

In difference form the constraint (5.2) is of the form,

$$\pm h_i^n\left(1-\frac{h_{i+1}^n-h_{i-1}^n}{2\Delta x}\right)>1. \quad (5.5)$$

Equation (5.3) can be written in the tridiagonal form

$$-h_{i+1}^{n+1}+\left(2+\frac{2\Delta x^2}{\Delta t\,H_i^n}\right)h_i^{n+1}-h_{i-1}^{n+1}=h_{i+1}^n-\left(2-\frac{2(\Delta x)^2}{\Delta t\,H_i^n}\right)h_i^n+h_{i-1}^n$$
$$+\frac{2(\Delta x)^2}{H_i^n}\left(\tfrac{23}{12}f_i^n-\tfrac{4}{3}f_i^{n-1}+\tfrac{5}{12}f_i^{n-2}\right), \quad (5.6)$$

where
$$H_i^n\equiv\frac{1}{3}\left\{(h_i^n)^3\pm\left(1-\frac{h_{i+1}^n-h_{i-1}^n}{2\Delta x}\right)^{-3}+\epsilon\right\}. \quad (5.7)$$

Because of (5.2), $H_i^n>\epsilon$ always and the tridiagonal matrix is well conditioned.

This scheme has a discretization error of $O((\Delta x)^2, (\Delta t)^2)$ and is stable for sufficiently small $\Delta t/\Delta x$.

We have tested the accuracy and stability of this scheme for two initial-value problems. In the first we use (2.15) with $\theta=0$ and the initial and boundary conditions $h(x,0)=\delta(x)$ and $h(\pm\infty,t)\to 0$. This equation governs the slow spreading of a thin sheet of Newtonian fluid on a plane (Batchelor 1967, p. 263). The exact solution is known to be of the similarity type (Landau & Lifshitz 1959, p. 195). In the second test we start with a permanent wave of §4 and find with the full equation (5.1) that the wave form remains the same for all times. Excellent agreement between numerical calculations and these solutions are found if $\Delta t/\Delta x\leqslant 0.05$ and $\epsilon\leqslant(\Delta t)^2$.

After solving for $h(x,t)$, we calculate h_0 from (2.20) and u_p from (2.18) with $z=h_0$. In the next sections two computed cases will be described: (1) flow due to upstream supply; (2) collapse of a fluid pile released over a layer of uniform depth.

In the first case a flux is added at $x=0$ from $t=0$ onwards. From (2.19) this implies a nonlinear relation between h and $\partial h/\partial x$ at $x=0$. In computations we use $h(0,t_{n-1})$ and $q(0,t_n)$ to compute $\partial h/\partial x$ at $(0,t_n)$ which then serves as the boundary value. For given initial data we first check the condition (5.5) and determine the domain of no flow and the domains in which the flow is of one direction. Equation (5.6) with appropriate signs is then invoked numerically to the next time step. This process is repeated for all later time steps.

6. Transient spreading of gravity currents

In each of the two examples to be discussed in this section, three uniform depths $h_\infty = 0.5$, 1, 1.5 will be taken as the initial states before disturbances are introduced. From (2.19) and (4.8) the supercritical depth ($h_\infty = 1.5$) is accompanied by a uniform flow with the discharge:

$$q_\infty = \tfrac{1}{3}(h_\infty - 1)^2(h_\infty + \tfrac{1}{2}). \tag{6.1}$$

For critical ($h_\infty = 1$) or subcritical ($h_\infty = 0.5$) depth, the starting state is one of no motion.

6.1. *Flow induced by upstream supply*

At $t = 0$ new fluid is suddenly introduced at the end $x = 0$; the rate of volume influx is kept constant at $q = 2$ for all $t > 0$. Surface profiles for three initial depths are shown in figure 9. The main conclusion is that the front eventually approaches a permanent wave. The local depth h increases from h_∞ at $x \sim \infty$ to a finite constant at $x = 0$. The final upstream depth can also be found from (6.1) to be $h(0, \infty) = 2.43$. The wave front has zero slope in the supercritical case, and is steep in the subcritical case, as is depicted in figure 5. The phase speeds of the wave front at large time $t = 8$ is 1.97, 1.40 and 1.03 corresponding respectively to $h_{\min} = 1.5$, 1.0 and 0.5 for the same $h_{\max} = 2.43$. These values are in excellent agreement with figure 4 obtained from (4.10) and (4.11). The evolution of h_0 and u_p are similar and are not presented here.

6.2. *Collapse of a fluid pile released over a layer of uniform depth*

Because of its possible relevance to the slow spreading of mud on a mountain slope or a seabed, we study the fate of a finite mud pile added to an otherwise uniform layer of depth h_∞. We present the transient solution for an initially triangular pile, i.e. the initial depth distribution is

$$h(x, 0) = \begin{cases} h_\infty + D\left(1 - \dfrac{|x|}{W}\right) & \text{if } |x| < W, \\ h_\infty & \text{if } |x| > W. \end{cases} \tag{6.2}$$

In the numerical example we have chosen $D = 1$ and $W = 2$. We have initially

$$1 - \frac{\partial h}{\partial x} = 1 + \frac{D}{W} = \frac{3}{2}$$

for the front face of the pile. The value of $1/h$ is minimum ($1/(h_\infty + D)$) at the peak and maximum ($1/h_\infty$) at the toes of the pile. We then check the value of $1/h$ against (2.21) to see whether the front will start to move. For $h_\infty = 1.8$ and 1.5, the entire pile front will start to move downward. But for the shallowest layer ($h_\infty = 0.5$) only a part of the front ($0 < x < 1$) will move downward at $t = 0$. The back of the pile does not move in all three cases at $t = 0$. The time evolution of the free surface is shown in figure 10. For the supercritical case $h_\infty = 1.5$ where the undisturbed layer is flowing, there is mud piling over the back face in the beginning, while the front is swept downward and the peak is lowered. The entire surface flattens out relatively quickly. For the critical case, there is no piling on the back, and the front also flattens, though rather slowly. In the supercritical case where the undisturbed mud layer is at rest, the initial development is similar to the critical case. However, after a long time the mud motion slows down. The front of the mud surface approaches one of the threshold profiles of static equilibrium corresponding to curve (*b*) in figure 2 without complete flattening.

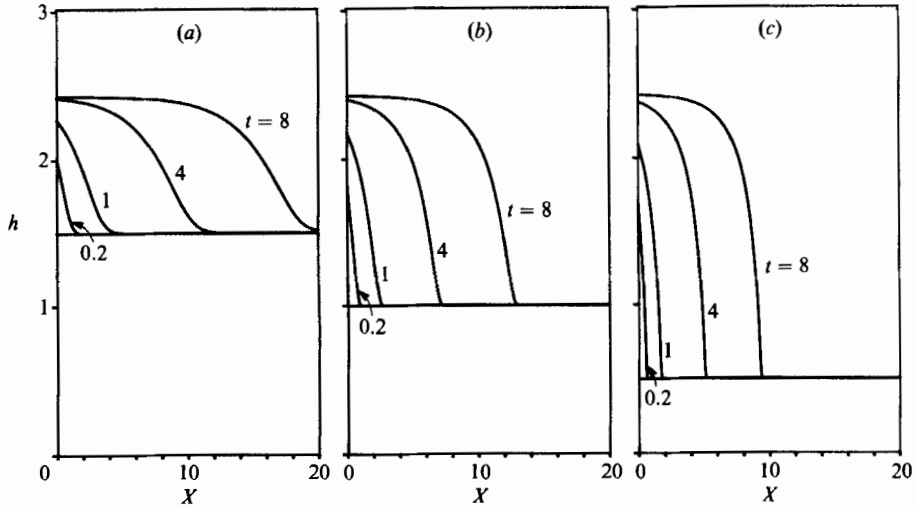

FIGURE 9. Evolution of mud surface due to a constant upstream discharge. (*a*) $h_\infty = 1.5$ (supercritical), (*b*) $h_\infty = 1.0$ (critical), (*c*) $h_\infty = 0.5$ (subcritical).

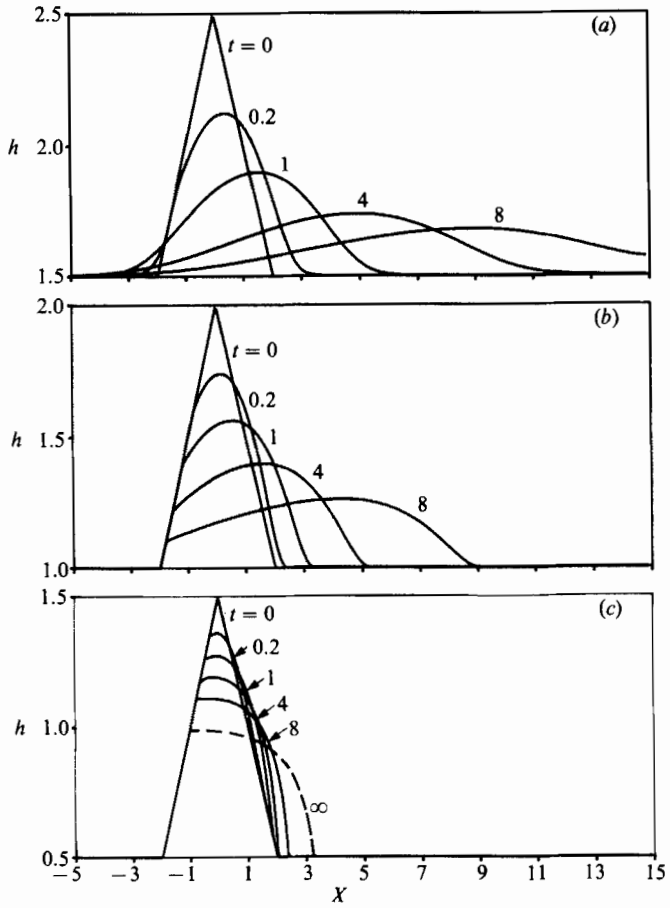

FIGURE 10. Collapse of a finite mud pile on a uniform layer. (*a*) $h_\infty = 1.5$ (supercritical), (*b*) $h_\infty = 1.0$ (critical), (*c*) $h_\infty = 0.5$ (subcritical).

In view of the last result, it is interesting to estimate analytically the ultimate dimensions of a mud pile released over a subcritical layer. This can be found by asserting that the final front must be at the threshold of static equilibrium (cf. §3) and by invoking mass conservation. For analytical simplicity the initial profile of (6.2) is again chosen, but other shapes have been found to give very similar results.

On the back face the initial slope is D/W. Therefore from (2.21) if

$$\frac{1}{h_\infty+D} > 1-\frac{D}{W} > -\frac{1}{h_\infty+D} \tag{6.3}$$

the back face will not move initially. Subsequent spreading of the front will flatten the peak of the pile. The ultimate profile on the back is therefore

$$h = h_\infty + D\left(1+\frac{x}{W}\right), \quad -W < x < x_\mathrm{m}. \tag{6.4}$$

On the front face, it must be given by (3.3):

$$h-h_\infty+\ln\frac{1-h}{1-h_\infty} = x-x_+, \quad x_\mathrm{m} < x < x_+. \tag{6.5}$$

The final positions of the peak x_m and of the front toe x_+ are still unknown. The depth h_m at x_m can be found from (6.4).

$$h_\mathrm{m} = h_\infty + D\left(1+\frac{x_\mathrm{m}}{W}\right). \tag{6.6}$$

Applying (6.5) to $h = h_\mathrm{m}$ at x_m and then eliminating h_m by using (6.6), we obtain a relation for x_m and x_+:

$$D\left(1+\frac{x_\mathrm{m}}{W}\right)+\ln\frac{1-h_\infty-D\left(1+\frac{x_\mathrm{m}}{W}\right)}{1-h_\infty} = x_\mathrm{m}-x_+. \tag{6.7}$$

By mass conservation, the final volume of the pile must be equal to the initial volume:

$$V = WD = \int_{-W}^{x_+}(h-h_\infty)\,\mathrm{d}x = \int_{-W}^{x_\mathrm{m}}(h-h_\infty)\,\mathrm{d}x+\int_{x_\mathrm{m}}^{x_+}(h-h_\infty)\,\mathrm{d}x. \tag{6.8}$$

If (6.4) is used in the first integral above, and (6.5) in the second, we get

$$\left[\frac{1}{2}\left(1-\frac{D}{W}\right)(h_\infty-h_\mathrm{m})-1\right](h_\mathrm{m}-h_\infty)-(1-h_\infty)\ln\frac{1-h_\mathrm{m}}{1-h_\infty} = WD, \tag{6.9}$$

which can be solved numerically for h_m. Afterwards, x_m can be calculated from (6.6) and x_+ from (6.7).

Variations of the final extent $L = x_+ + W$ and of the final pile height h_m are plotted in figures 11 and 12 respectively for various V and h_∞. Note that for a given h_∞ a new mud pile will spread at the base only if V exceeds a certain minimum. Otherwise there can be only a local flattening near the peak of the initial pile but no spreading at the base. These thresholds fall on the chain line in figure 11. On a layer with a larger h_∞, a pile with a relatively small V will spread at its base. The final spread L of course increases with V and h_∞. Similarly for a pile on a layer of given h_∞ to lower its peak height h_m and to yield at its base, V must also exceed a threshold, which is indicated by the chain line in figure 12. The final values of h_m are smaller for smaller V but for larger h_∞.

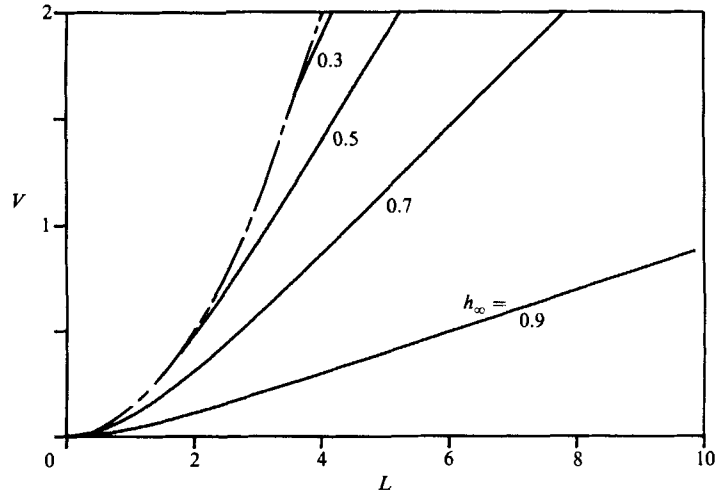

FIGURE 11. The final extent L of spreading of a mud pile as a function of V and h_∞. The chain line gives the minimum V below which the pile base on a given h_∞ does not spread; mud motion is localized near the peak.

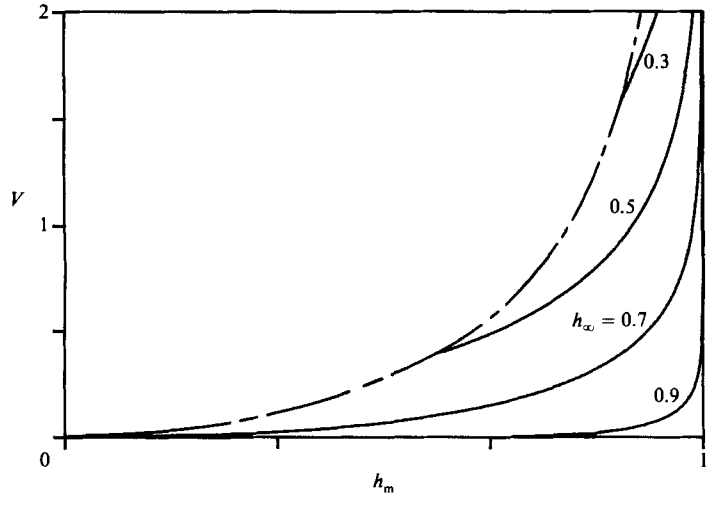

FIGURE 12. The final pile height as a function of V and h_∞. The chain line gives the minimum V below which the mud pile base does not move.

7. Response to an external pressure over a horizontal layer

As a final class of examples we consider the effects of a pressure distribution of prescribed strength applied externally on the surface $z = h$. In the case of a muddy seabed the pressure distribution may be caused either by a stationary submarine object in a water current, or an object moving above and parallel to the mud–water interface.

Although we have studied the general case of a sloping layer, most of the new physics can be revealed by a pressure distribution over a horizontal layer. We shall

therefore only discuss the latter case. It is then more appropriate to replace the normalizations in (2.17) as follows, so that the limit of $\theta = 0$ is easily taken:

$$\left.\begin{aligned} \bar{h} &\to \frac{P_0}{\rho g \cos\theta}, \quad P \to P_0 P', \\ (x, W) &= \frac{P_0^2}{\rho g \tau_0}(x', W'), \\ C &= \frac{\tau_0^2 C'}{\rho g \mu \cos\theta}, \end{aligned}\right\} \tag{7.1}$$

where P_0 is the characteristic scale of the applied pressure. Eliminating h_0 and q from (2.14), (2.19) and (2.20), we obtain the dimensionless equations for h

$$h_t = \tfrac{1}{3}[h^3 \mp (\sigma - h_x - P_x)^{-3}](h_{xx} + P_{xx}) + h h_x[\pm\sigma - h(\sigma - h_x - P_x)], \tag{7.2}$$

where

$$\sigma = \frac{P_0 \tan\theta}{\tau_0}. \tag{7.3}$$

Again the primes are omitted for brevity. The flow is

$$\left\{\begin{matrix}\text{rightward} \\ \text{leftward}\end{matrix}\right\} \quad \text{if} \quad \sigma - h_x - P_x \left\{\begin{matrix} > \dfrac{1}{h} \\ < -\dfrac{1}{h} \end{matrix}\right\}. \tag{7.4}$$

We shall consider the initial conditions that

$$P = 0, \quad h = h_\infty = \text{constant} < 1, \quad t \leqslant 0. \tag{7.5}$$

Thus the mud layer is initially stationary.

The gradient of the pressure is chosen to be a cosine pulse which is applied instantly and moves at a constant velocity C parallel to the mud surface, i.e.

$$P_x = \left\{\begin{matrix} -\dfrac{\pi}{2W}\cos\left[\dfrac{\pi}{2W}(x - Ct)\right], & |x - Ct| < W, \\ 0, & \text{otherwise}, \end{matrix}\right\} \quad t > 0, \tag{7.6}$$

which is continuous everywhere and convenient for numerical integration. The numerical procedure described in §5 is easily modified for the present purposes. Note that mud motion is forced to start by the term

$$\tfrac{1}{3}(h_\infty^3 \pm (1 - P_x)^{-3}) P_{xx} \tag{7.7}$$

on the right-hand side of (7.2). Because both P_x and P_{xx} are present, the mud surface is usually not symmetric in x even if P_x is symmetric.

In the following examples we shall only discuss the horizontal layer, so that $\theta = \sigma = 0$.

7.1. *Stationary pressure* ($C = 0$)

In figure 13 the transient response to a suddenly applied, and then maintained, pulse of negative pressure gradient of cosine form is plotted for $W = 0.5$ and $h_\infty = 0.9$. Directly under this negative pressure gradient, mud is pushed to the right. By mass conservation, there must be a pile on the right and a trough on the left. As can be expected, some mud just outside the pressurized zone must also be moved. As t

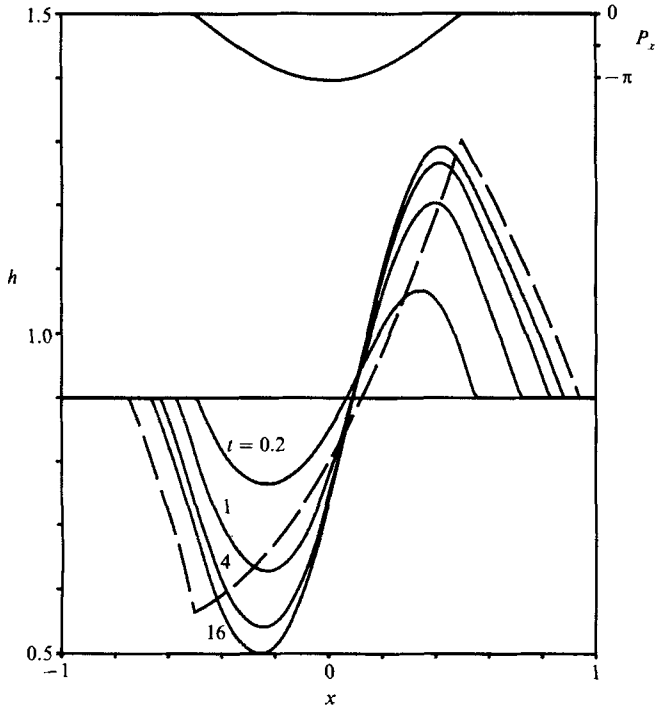

FIGURE 13. Transient evolution of the surface of a horizontal mud layer due to a stationary cosine pulse of pressure gradient. For comparison, the dashed line corresponds to the final surface due to a top-hat pulse with inverse pressure gradient $W/a = 0.5$.

increases, a final equilibrium state is reached.† Note that the profile is not symmetric in x, unlike the pressure gradient itself. The result for a positive pressure gradient can be obtained from the mirror reflection of figure 13 with respect to $x = 0$.

For further insight, it is useful to derive the final static profile analytically. The dimensionless governing equation is obtained from (7.4) by letting $\sigma = 0$ and changing the symbols from $>$ (or $<$) to $=$ if the mud is about to move to the right (or left). Unfortunately (7.6) does not permit analytical integration of (7.4). We therefore choose a top-hat (discontinuous) pressure gradient pulse where $\mathrm{d}P/\mathrm{d}x$ is a negative constant $-a/W$ within $|x| < W$ with $a > W/h_\infty$. Equation (7.4) then gives

$$-\frac{\mathrm{d}h}{\mathrm{d}x} = \begin{cases} -a/W + 1/h, & |x| < W, \quad (7.8a) \\ 1/h, & |x| > W, \quad (7.8b) \end{cases}$$

With $h = h_{\max}$ at $x = W$, (7.8a) can be integrated to

$$a(h_{\max} - h) - W \ln \frac{W - ah}{W - ah_{\max}} = \frac{a^2}{W}(W - x), \quad (-W < x < W). \tag{7.9}$$

The resulting mud depth h is monotonic in x. Within the pressurized zone, mud is pushed to the right, the minimum depth must occur at the edge $x = -W$, so that

$$a(h_{\max} - h_{\min}) - W \ln \frac{W - ah_{\min}}{W - ah_{\max}} = 2a^2. \tag{7.10}$$

† Considerable computing time is needed to reach this state.

By gravity the mud surface adjacent to but outside the pressurized zone must also be deformed and assumes the rightward-facing threshold profile given by the dimensionless form of (31), i.e.

$$h^2-h_{\min}^2 = -2(x+W), \quad x_{\min} < x < -W, \tag{7.11a}$$

$$h^2-h_{\max}^2 = -2(x-W), \quad W < x < x_{\max}. \tag{7.11b}$$

Furthermore, outside $x_{\min} < x < x_{\max}$ the mud surface is again flat so that $h = h_\infty$ and

$$x_{\max} = W+\tfrac{1}{2}(h_{\max}^2-h_\infty^2); \quad x_{\min} = -W-\tfrac{1}{2}(h_\infty^2-h_{\min}^2). \tag{7.12a,b}$$

Thus the only unknowns are $h_{\max}$ and $h_{\min}$. Invoking mass conservation we must have

$$\int_{x_{\min}}^{-W} + \int_{-W}^{W} + \int_{W}^{x_{\max}} (h-h_\infty)\,dx = 0. \tag{7.13}$$

Substituting (7.11*a*) in the first integral, (7.9) in the second, (7.11*b*) in the third, and using (7.10), we find

$$\tfrac{1}{3}(h_{\max}^3-h_{\min}^3)-\frac{1}{2}\left(h_\infty-\frac{W}{a}\right)(h_{\max}^2-h_{\min}^2)-2W\left(h_\infty-\frac{W}{a}\right) = 0. \tag{7.14}$$

Equations (7.10) and (7.14) can be solved for $h_{\max}$ and $h_{\min}$ numerically as a function of W/a, a and h_∞. The static profile is also plotted in figure 13 for comparison with the transient profiles due to a cosine pulse of equal total strength. There is a gross similarity between the results of the two pressure pulses.

The advantage of the top hat is that (7.14) can be used to find easily the dependence of $h_{\max}$ and $h_{\min}$ on the gross features of the pressure pulse a, and W/a which is the reciprocal of the pressure gradient pulse. The results are plotted in figure 14 for $h_\infty = 0.9$. For the same pressure amplitude a, increasing W decreases the pressure gradient, hence reduces the mud deformation $h_{\max}-h_{\min}$. For the same pressure gradient, or W/a, increasing a increases the mud deformation. The values of $x_{\max}$ and $x_{\min}$ can then be obtained from (7.12*a*, *b*). Since the mud surface can be deformed only if $W/a < h_\infty$, it must remain flat beyond the chain line $W/a = h_\infty$ in figure 14. Near $W = 0$, it can be shown that $\frac{3}{2}h_\infty > h_{\max} > h_{\min} > W/a$. While (7.9) indicates that the mud pile becomes a line with height no more than $\frac{3}{2}h_\infty$ but zero width, the corresponding limit of the pressure gradient is too large and thus invalidates our theory.

We have compared these final-state results to the large-time values of $h_{\max}$ and $h_{\min}$ in a few of the transient calculations for the negative cosine pulse and found them to be close, if a is taken to be unity so that the averaged pressure gradient is the same in both cases.

7.2. *Moving pressure*

In figures 15 and 16, the mud evolution is plotted for $C = 1$ and $C = -1$, respectively. The initial development is similar to the case of $C = 0$. Since a negative pressure gradient pushes mud to the right, the rightward-moving pulse produces a larger pile than the leftward-moving pulse at later times. For the right-going pressure in figure 15, the pile finally reaches a steady state. Only the back face of the pile is forced directly by the pressure gradient above, while the front part of the pile is unforced. More interestingly, a permanent trough is left behind on the left, as a consequence of mass conservation. For the left-going pressure in figure 16, a steady trough follows the moving pressure to the left, leaving a permanent pile of relatively small size on the right. These permanent footprints owe their existence to the Bingham yield

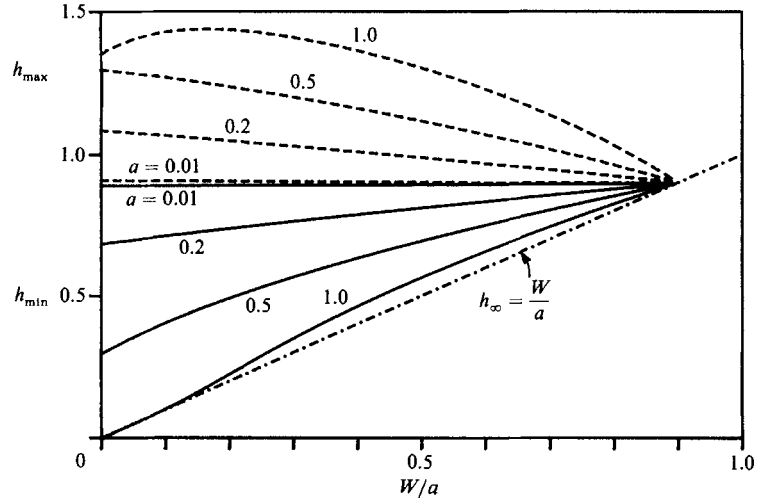

FIGURE 14. The final heights of peak (dashed curves) and trough (solid curves) of the mud surface as function of a and W/a (reciprocal of dimensionless pressure gradient) for $h_\infty = 0.9$. The chain line represents the point $W/a = h_\infty$ beyond which there is no mud motion.

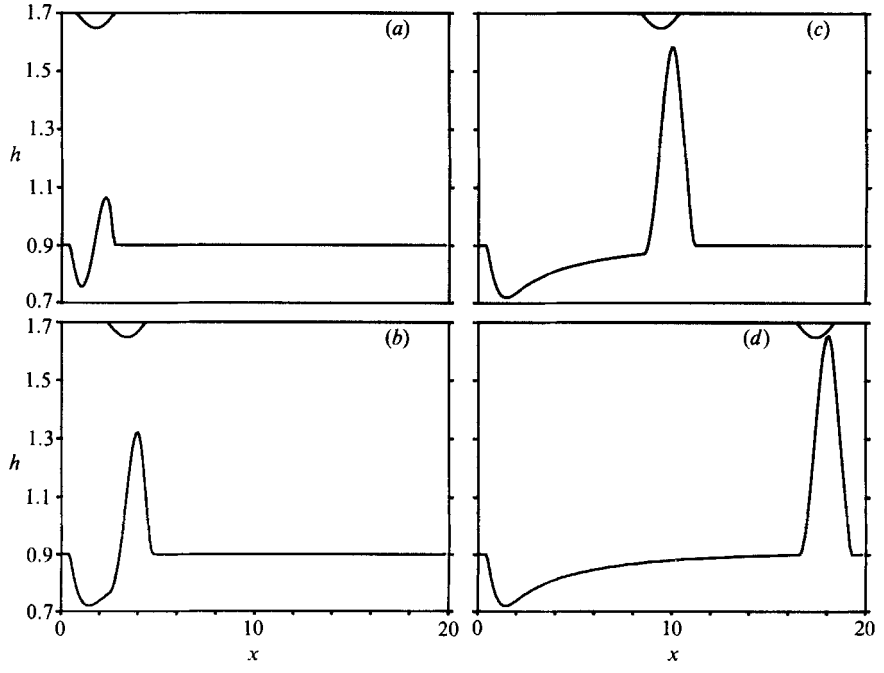

FIGURE 15. Transient evolution of the surface of a horizontal mud layer due to a pressure gradient pulse moving to the right, as shown at the top of each plot. $C = 1$ and $h_\infty = 0.9$. (*a*) $t = 0.2$, (*b*) $t = 1.0$, (*c*) $t = 4.0$, (*d*) $t = 8.0$.

stress. Note that the moving trough cannot be accompanied by new piling in its vicinity, otherwise the volume of the pile left behind would increase without bound and no steady state would be possible. Again owing to nonlinearity and the presence of both P_x and P_{xx} in the governing equation, the surface profiles in figures 15 and 16 are clearly different and asymmetric in x in both cases. If the sign of the pressure

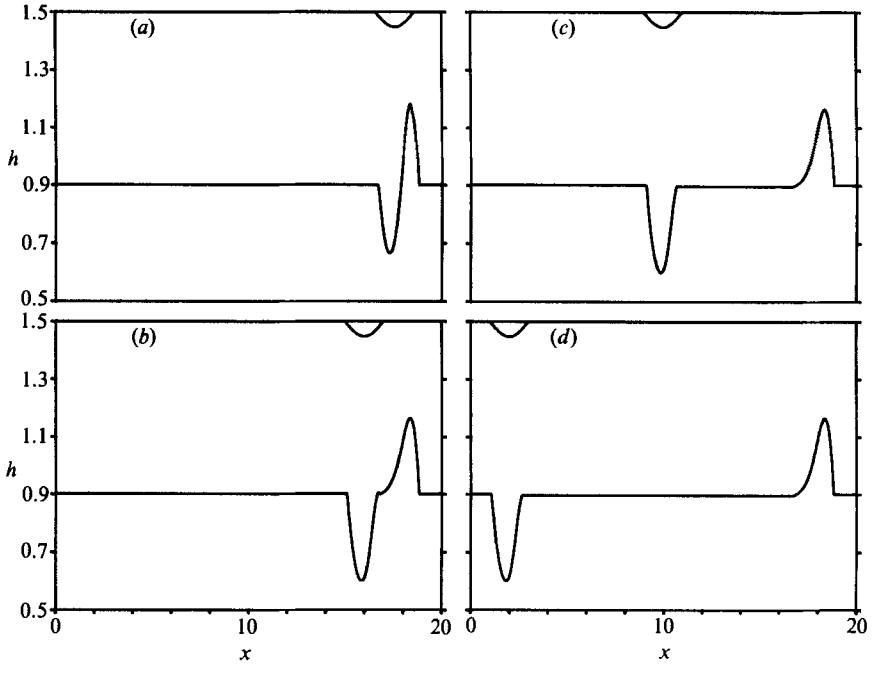

FIGURE 16. Transient evolution of the surface of a horizontal mud layer due to a pressure gradient pulse moving to the left. $C = -1$ and $h_\infty = 0.9$. (*a*) $t = 0.2$, (*b*) $t = 1.0$, (*c*) $t = 4.0$, (*d*) $t = 8.0$.

gradient is reversed in both cases, the response curves are interchanged; i.e. the response to a negative pulse moving to the right is the mirror image of the response to a positive pulse moving to the left, and vice versa.

Without further computations, the results obtained so far can be used to infer qualitatively the mud response beneath a wide two-dimensional cylinder which has a flat keel and is moving parallel to but above a horizontal mud layer immersed at the sea bottom. Let the cylinder move from left to right. As x increases, the pressure below the keel first drops around the stern and then rises near the bow. Hence the pressure gradient is a positive pulse near the bow and a negative pulse near the stern. Near the bow, there would at first be a moving mud trough; a stationary pile is left behind. But the pile caused by and moving with the stern soon catches up and swallows the stationary pile created by the bow. A larger trough is left behind the stern. These features are indeed found in numerical experiments not presented here.

The presence of either a trough or a pile left behind a moving disturbance suggests that the direction and the speed of an underwater object moving near a muddy sea bed can be estimated long after its departure. The footprint of course depends on the size, the shape and the speed of the object and the bed slope. In particular, an object creates a relatively large and long footprint if it moves *down* the slope. This has also been confirmed numerically.

8. Summary

Based on a shallow-water approximation similar to the theory of lubrication, a theory has been given for slow flows of a sheet of Bingham-plastic fluid on a plane bed. Static profiles with non-uniform depth are first found which correspond to

thresholds of incipient flow. Because of the yield stress, these profiles can exist on a sloping bed. In contrast, in a Newtonian fluid, the state of static equilibrium with finite depth is possible only when the bed is horizontal and depth constant. Furthermore, a variety of gravity currents are found, some of which can propagate up the slope and may correspond to the rise of a mud reservoir.

For the transient start of a steady discharge of fresh mud, the front of the mud current is found to reach a permanent form advancing at a constant wave speed. When a finite mass is added to a uniform layer of stationary fluid on a slope, the flow stops after spreading over a finite extent. The extent can be predicted by invoking mass conservation and requiring that the final profile corresponds to a threshold static equilibrium. This result is relevant to the final stage of a mud slide. Lastly, a moving external pressure, which may be caused by a moving body above the muddy sea bed, can leave a permanent footprint on the mud surface. Further studies, especially for two-dimensional pressure distributions, may enable one to estimate the size, shape and speed of a submarine object by its footprint.

Within the framework of a Bingham-plastic model, other studies are needed. For example, a ship navigating a poorly dredged channel may experience large resistance by giving up energy to dissipation in the bottom mud. If the sea bed is covered with a thick layer of fluid mud, the mud/water interface need not be horizontal when in static equilibrium. Consequently, internal waves may exist on an inclined interface. Finally, the effect of vertical variation of clay concentration may affect the viscosity and yield stress, hence must be important in the dynamics of fluid mud.

The Bingham model is of course still an idealization for fluid mud which is, strictly speaking, a pseudo-plastic with a smooth variation between stress and strain. Certain predictions made here are expected to require refinement if a more accurate constitutive relation is given. For example, the footprint left behind a departed submarine object may disappear after a very long time. As clay concentration increases, a viscoelastic-plastic, and possibly thixotropic, model may be more appropriate. More theoretical and experimental work would be worthwhile.

We thank the US Office of Naval Research, Ocean Engineering Division for financial support through contract No. 00014-83-K-0550, NR 294-095. Part of the final version was written while C.C.M. was visiting l'Institut de Mécanique de Grenoble, France.

REFERENCES

BATCHELOR, G. K. 1967 *Introduction to Fluid Dynamics*. Cambridge University Press.

BENJAMIN, T. B. 1957 Wave formation in a laminar flow down an inclined plane. *J. Fluid Mech.* **2**, 554–574.

BENNEY, D. J. 1966 Long waves on liquid films. *J. Maths Phys.* **45**, 150–155.

BERCOVIER, M. & ENGELMAN, M. 1980 The finite element method for incompressible non-Newtonian flows. *J. Comput. Phys.* **36**, 313–326.

BIRD, R. B., ARMSTRONG, R. C. & HASSAGER, O. 1987 *Dynamics of Polymeric Liquids, Vol. 1. Fluid Mechanics*. Wiley.

BIRD, R. B., DAI, G. C. & YARUSSO, B. J. 1983 The rheology and flow of viscoplastic materials. *Rev. Chem. Engng* **1**, 1–70.

CROCHET, M. J., DAVIES, A. U. & WALTERS, K. 1984 *Numerical Simulation of Non-Newtonian Flow*. Elsevier.

CROCHET, M. H. J. & WALTERS, K. 1983 Numerical methods in non-Newtonian fluid mechanics. *Ann. Rev. Fluid Mech.* **15**, 241–260.

DIDDEN, N. & MAXWORTHY, T. 1982 The viscous spreading of plane and axisymmetric gravity currents. *J. Fluid Mech.* **121**, 27–42.

HUPPERT, H. E. 1982*a* The propagation of two-dimensional and axisymmetric viscous gravity currents over a rigid horizontal surface. *J. Fluid Mech.* **121**, 43–58.

HUPPERT, H. E. 1982*b* Flow and instability of a viscous current down a slope. *Nature* **300**, 427–429.

HUPPERT, H. E. 1986 The intrusion of fluid mechanics into geology. *J. Fluid Mech.* **173**, 557–594.

KRONE, R. B. 1963 A study of rheological properties of estuarial sediments. *Ser. Rep.* 63–8. Hydraulic Engineering Laboratory and Sanitary Research Laboratory, University of California, Berkeley.

LANDAU, L. D. & LIFSHITZ, E. M. 1959 *Fluid Mechanics*, p. 195. Pergamon.

LIN, S. P. 1969 Finite-amplitiude stability of a parallel flow with a free surface. *J. Fluid Mech.* **36**, 112–126.

LIN, S. P. 1974 Finite-amplitude side-band stability of a viscous film. *J. Fluid Mech.* **63**, 417–429.

MCPHERSON, H. 1980 The attenuation of water waves over a non-rigid bed. *J. Fluid Mech.* **97**, 721–742.

MAKAROV, A. M. & SAL'NIKOV, V. G. 1972 Nonstationary shear flow of viscoplastic medium. *J. Appl. Mech. Tech. Phys.* **13**, 546–550.

MAKAROV, A. M., ZHDANOVA, L. A. & PLOLZOVA, O. N. 1974 Nonsteady state flow of a viscoplastic medium in a plane channel. *J. Engng Phys.* **22**, 51–55.

MEHTA, A. J. & MAA, P. Y. 1987 Mud erosion by waves: a laboratory study. *Continental Shelf Res.* **7**, 1268–1284.

MEI, C. C. 1966 Nonlinear gravity waves in a thin sheet of viscous fluid. *J. Maths. Phys.* **45**, 266–288.

MEI, C. C. & LIU, K. F. 1987 A Bingham-plastic model for a muddy seabed under long waves. *J. Geophys. Res.* **92**, 14587–14594.

MIGNIOT, P. C. 1968 Étude de propriétés physiques de différents sediments tres fins et de leur comportment sous des action hydrodynamiques. *La Houille Blanche* **7**, 591–620.

PHAN-THIEN, N. 1983 A similarity solution for a Rayleigh flow of a Bingham fluid. *Trans. ASME* E: *J. Appl. Mech.* **50**, 229–230.

VERREET, G. & BERLAMONT, J. 1987 Rheology and non-Newtonian behavior of sea and estuarine mud. *Encyclopedia of Fluid Mechanics*, vol. 7 (ed. N. Cheremissinoff). Gulf.

WANG, M. F., DUAN, W. Z., TAN, Z. M. & ZHAN, Y. Z. 1985 On the structure and movement mechanism of flow with hyperconcentration of sediments. *Proc. Intl. Workshop on Flow of Hyperconcentrated Sediments*. Beijung, China.

WILLIAMS, D. J. A. 1980 Rheology of cohesive suspensions. In *Estuarine Cohesive Sediment Dynamics* (ed. A. J. Mehta), pp. 110–125. Springer.

YIH, C. S. 1954 Stability of parallel laminar flow with a free surface. *Proc. 2nd Cong. Appl. Mech.* pp. 623–628.

YIH, C. S. 1963 Stability of liquid flow down an inclined plane. *Phys. Fluids* **6**, 321–334.